Available online at www.sciencedirect.com
ScienceDirect
Physics Letters A 366 (2007) 289–297
PHYSICS LETTERS A
www.elsevier.com/locate/pla

Tachyonic spectral map of a binary pulsar

Roman Tomaschitz *

Department of Physics, Hiroshima University, 1-3-1 Kagami-yama, Higashi-Hiroshima 739-8526, Japan

Received 7 January 2007; accepted 29 January 2007

Available online 21 February 2007

Communicated by V.M. Agranovich

Abstract

We study tachyonic synchrotron densities of ultra-relativistic electrons in helical motion. There is a longitudinally polarized spectral component due to the negative mass square of the superluminal quanta. The helical pitch-angle scaling of the transversal and longitudinal spectral densities is investigated, in particular the transition from circular to rectilinear motion. The magnetic field induces oscillations along the power-law slopes of the superluminal radiation densities, whose amplitude depends on the pitch angle. At moderate field strength and ultra-relativistic orbital speed, the modulations are tiny, but they become quite pronounced in the surface fields of γ-ray pulsars, resulting in cockscomb distributions. A tachyonic spectral fit to the γ-ray flux of the binary pulsar PSR B1259–63 is performed. The γ-ray wideband of this millisecond pulsar is reproduced by a tachyonic cascade spectrum, capable of generating the spectral curvature in double-logarithmic plots as well as the extended spectral plateau defined by ISGRI, OSSE, COMPTEL, and EGRET flux points.

PACS: 41.60.Ap; 03.50.Kk; 95.30.Gv; 97.60.Gb

Keywords: Tachyonic synchrotron radiation; Superluminal curvature radiation; Longitudinal polarization; Cascade spectra; Pulsar magnetospheres

1. Introduction

We investigate tachyonic synchrotron emission from electrons in pulsar magnetospheres. The goal is to provide quantitative evidence for this radiation by working out a specific example, a tachyonic spectral fit to the γ-ray spectrum of the binary pulsar PSR B1259–63 orbiting around the massive Be star SS 2883. When tachyonic spectral densities are averaged with thermal or power-law electron densities, this leads to cascade spectra [1,2], extended spectral plateaus followed by power-law decay terminating in exponential decay. A glance at the spectral map of PSR B1259–63 suggests that it can readily be fitted by a cascade spectrum.

In Section 2, the tachyonic spectral densities of electrons in helical orbits and their pitch-angle scaling are derived. In Section 3, we discuss the pitch-angle averaging and its effect on modulations along the spectral slopes induced by the negative mass-square of the radiation field. In particular, we illustrate the helical cross-over from circular orbits to rectilinear motion in the surface magnetic field of a γ-ray pulsar. In Section 4, we average the tachyonic spectral densities with electronic source populations and perform a wideband fit to the PSR B1259–63/SS 2883 binary system, ranging from high-energy X-rays to TeV γ-rays. In Section 5, we present our conclusions.

We consider electrons in a constant magnetic field $\mathbf{B} = (0,0,B)$, $B>0$. The equations of motion read $d(\gamma m\mathbf{v})/dt = e\mathbf{v}\times\mathbf{B}$. The helical orbits can be parametrized as

$$\mathbf{x}(t) = \left(-\frac{\upsilon_\perp}{\omega_\mathrm{B}}\,\mathrm{sign}(e)\cos(\omega_\mathrm{B}t), \frac{\upsilon_\perp}{\omega_\mathrm{B}}\sin(\omega_\mathrm{B}t), \upsilon_\parallel t\right),$$
$$\omega_\mathrm{B} := |e|B/(m\gamma),\ \upsilon_\perp := \upsilon\sin\alpha,\ \upsilon_\parallel := \upsilon\cos\alpha, \tag{1}$$

where α is the pitch angle between $\mathbf{B}$ and $\mathbf{v}$, $0\leqslant\alpha\leqslant\pi$. The speed υ along the orbit is constant. A pitch angle of $\pi/2$ gives circular orbits in the (x,y)-plane, and $\alpha=0$ or π means straight uniform motion. We put $\hbar=c=1$, and use the Heaviside–Lorentz system. The electric charge e is defined negative for electrons, γ is the Lorentz factor, and m the electron

* Tel.: +81 824 247361; fax: +81 824 240717.
E-mail address: tom@geminga.org.

0375-9601/$ – see front matter
doi:10.1016/j.physleta.2007.01.084

mass. We also admit $\mathrm{sign}(e) = 0$ in (1), that is, planar transversal oscillations, realizable by undulators in storage rings [3–8].

2. Superluminal radiation densities

2.1. High-frequency regime

The tachyonic radiation theory pertinent to a charge in arbitrary motion has been given in Ref. [1]. The multipole expansion of the superluminal Poynting vectors is summarized in Eqs. (2)–(4). We introduce polar coordinates with $\mathbf{B}$ as polar axis and polar angle θ, and consider the tachyonic wave vector in the (y,z)-plane, so that $\mathbf{k} := k(\omega)\mathbf{n}$, $\mathbf{n} = (0, \sin\theta, \cos\theta)$. Wave number and frequency are related by the superluminal dispersion relation, $k(\omega) = \sqrt{\omega^2 + m_\mathrm{t}^2}$, where m_t is the mass of the tachyonic quanta. The sign convention is $m_\mathrm{t}^2 > 0$, so that the plus-sign in the dispersion relation implies a negative mass square. We define two transversal polarization vectors, $\boldsymbol{\varepsilon}_\parallel := (0, -\cos\theta, \sin\theta)$, and $\boldsymbol{\varepsilon}_\perp := \boldsymbol{\varepsilon}_\parallel \times \mathbf{n}$, so that $\mathbf{n}$, $\boldsymbol{\varepsilon}_\parallel$ and $\boldsymbol{\varepsilon}_\perp$ constitute an orthonormal triad, $\boldsymbol{\varepsilon}_\parallel = -\boldsymbol{\varepsilon}_\perp \times \mathbf{n}$. We study the ultra-relativistic limit, $\gamma \gg 1$.

The angular-integrated power radiated in the nth harmonic can readily be assembled from Eqs. (2.27), (2.28) and (2.31) of Ref. [1],

$$P_n^\mathrm{T} \approx \alpha_\mathrm{q} \int_0^\pi \frac{k_n^2 \omega_n}{\beta_n} \bigl|\boldsymbol{\lambda}_n^\mathrm{T}(z_n)\bigr|^2 \sin\theta\, d\theta,$$

$$P_n^\mathrm{L} \approx \alpha_\mathrm{q} m_\mathrm{t}^2 \int_0^\pi \frac{k_n^2}{\beta_n \omega_n} \bigl|\boldsymbol{\lambda}_n^\mathrm{L}(z_n)\bigr|^2 \sin\theta\, d\theta. \tag{2}$$

Here, $\alpha_\mathrm{q} = q^2/(4\pi\hbar c) \approx 1.0 \times 10^{-13}$ is the tachyonic fine structure constant. The superluminal radiation field, a Proca field with negative mass square, is coupled by minimal substitution to the subluminal current, and q is the tachyonic charge of the source particle. The tachyon mass is $m_\mathrm{t} \approx 2.15\ \mathrm{keV}/c^2$. These estimates are obtained from hydrogenic Lamb shifts [9]. The tachyonic frequencies and wave numbers in (2) read

$$\omega_n := \frac{n\omega_\mathrm{B} + \upsilon_\parallel \beta_n \cos\theta}{1 - \upsilon_\parallel^2 \cos^2\theta},$$

$$\beta_n := \sqrt{n^2\omega_\mathrm{B}^2 + m_\mathrm{t}^2\bigl(1 - \upsilon_\parallel^2 \cos^2\theta\bigr)},$$

$$k_n := k(\omega_n) = \frac{\omega_n - n\omega_\mathrm{B}}{\upsilon_\parallel \cos\theta} = \frac{n\omega_\mathrm{B}\upsilon_\parallel \cos\theta + \beta_n}{1 - \upsilon_\parallel^2 \cos^2\theta}. \tag{3}$$

The squared multipole coefficients can be calculated in closed form [1],

$$\bigl|\boldsymbol{\lambda}_n^\mathrm{T}(z_n)\bigr|^2 = \bigl(\upsilon_\parallel \sin\theta - (n/z_n)\upsilon_\perp \cos\theta\bigr)^2 J_n^2(z_n) + \mathrm{sign}^2(e)\upsilon_\perp^2 J_n'^2(z_n),$$

$$\bigl|\boldsymbol{\lambda}_n^\mathrm{L}(z_n)\bigr|^2 = \bigl((n/z_n)\upsilon_\perp \sin\theta + \upsilon_\parallel \cos\theta\bigr)^2 J_n^2(z_n),$$

$$z_n := k_n \frac{\upsilon_\perp}{\omega_\mathrm{B}} \sin\theta. \tag{4}$$

We refrain from writing $\mathrm{sign}^2(e) = 1$, since in this way the contributions of the two linear transversal polarizations (defined by $\boldsymbol{\varepsilon}_{\parallel,\perp}$) to the radiated power can easily be distinguished; the term stemming from the $\boldsymbol{\varepsilon}_\perp$-polarized component of the radiation field has the $\mathrm{sign}^2(e)$-factor attached. Moreover, by putting $\mathrm{sign}^2(e) = 0$ in (4), we find the transversal power radiated by oscillating charges in undulator fields. The electromagnetic counterpart of (2)–(4) is recovered in the limit of vanishing tachyon mass [10].

The integrals $P_n^{\mathrm{T,L}}$ in (2) give the power transversally or longitudinally radiated in the harmonic ω_n. We are interested in the large-n asymptotics,

$$\omega_n = \frac{n\omega_\mathrm{B}}{1 - \upsilon_\parallel \cos\theta}\left(1 + \frac{1}{2}(1 - \upsilon_\parallel \cos\theta)\upsilon_\parallel \cos\theta \frac{m_\mathrm{t}^2}{n^2\omega_\mathrm{B}^2} + \mathrm{O}\left(\frac{1}{n^4}\right)\right), \tag{5}$$

the expansion parameter is $m_\mathrm{t}^2/(n\omega_\mathrm{B})^2$. The $1/n^2$-expansion of the wave numbers reads

$$k_n = \frac{n\omega_\mathrm{B}}{1 - \upsilon_\parallel \cos\theta}\left(1 + \frac{1}{2}(1 - \upsilon_\parallel \cos\theta)\frac{m_\mathrm{t}^2}{n^2\omega_\mathrm{B}^2} + \cdots\right), \tag{6}$$

and the argument z_n of the Bessel functions in (4) is expanded as

$$\frac{z_n(\theta)}{n\upsilon_\perp} = \frac{\sin\theta}{1 - \upsilon_\parallel \cos\theta} + \frac{1}{2}\sin\theta \frac{m_\mathrm{t}^2}{n^2\omega_\mathrm{B}^2} + \mathrm{O}\left(\frac{1}{n^4}\right). \tag{7}$$

In (2), we expand the integrands in $\theta - \theta_\mathrm{c}$, at the stationary phase, $dz_n(\theta_\mathrm{c})/d\theta = 0$, which reads

$$\cos\theta_\mathrm{c} = \upsilon_\parallel\left(1 - \frac{1}{2}\frac{m_\mathrm{t}^2}{n^2\omega_\mathrm{B}^2}\bigl(1 - \upsilon_\parallel^2\bigr)^2 + \mathrm{O}\left(\frac{1}{n^4}\right)\right). \tag{8}$$

Hence,

$$\frac{z_n}{n\upsilon_\perp} = \frac{1}{\sqrt{1 - \upsilon_\parallel^2}}\left(1 + \frac{1}{2}\frac{m_\mathrm{t}^2}{n^2\omega_\mathrm{B}^2}\bigl(1 - \upsilon_\parallel^2\bigr)\right) - \frac{1}{2}\frac{(\theta - \theta_\mathrm{c})^2}{(1 - \upsilon_\parallel^2)^{3/2}}\left(1 + \mathrm{O}\left(\frac{1}{n^2}\right)\right) + \mathrm{O}\left((\theta - \theta_\mathrm{c})^3, \frac{1}{n^4}\right). \tag{9}$$

We introduce a new integration variable ψ in (2),

$$\theta - \theta_\mathrm{c} = \varepsilon\psi, \quad \varepsilon := \sqrt{\frac{1}{\gamma^2} - \frac{m_\mathrm{t}^2}{n^2\omega_\mathrm{B}^2}\sin^4\alpha}, \tag{10}$$

where $\gamma = (1 - \upsilon^2)^{-1/2} \gg 1$, and approximate

$$\sin\theta\, d\theta \approx \varepsilon \sin\alpha\, d\psi, \qquad 2\left(1 - \frac{z_n}{n}\right) \approx \frac{\varepsilon^2}{\sin^2\alpha}\bigl(1 + \psi^2\bigr). \tag{11}$$

In the vicinity of θ_c, the $|\boldsymbol{\lambda}_n^{\mathrm{T,L}}|^2$-factors in (4) can be replaced by

$$\bigl|\boldsymbol{\lambda}_n^\mathrm{T}(z_n)\bigr|^2 \approx \varepsilon^2\psi^2 J_n^2(z_n) + \mathrm{sign}^2(e)\sin^2\alpha J_n'^2(z_n),$$

$$\bigl|\boldsymbol{\lambda}_n^\mathrm{L}(z_n)\bigr|^2 \approx J_n^2(z_n), \tag{12}$$

and the Bessel functions in (12) by their Nicholson approximation. The latter applies for large positive n and z, so that $z/n \approx 1$ and $z < n$,

$$J_n(z) \approx \frac{1}{\sqrt{3}\pi}\left(2\left(1-\frac{z}{n}\right)\right)^{1/2} K_{1/3}(\lambda),$$
$$J_n'(z) \approx \frac{2}{\sqrt{3}\pi}\left(1-\frac{z}{n}\right) K_{2/3}(\lambda),$$
$$\lambda := \frac{n}{3}\left(2\left(1-\frac{z}{n}\right)\right)^{3/2}. \tag{13}$$

In the preceding notation, this means

$$J_n(z_n) \approx \frac{1}{\sqrt{3}\pi}\frac{\varepsilon}{\sin\alpha}\sqrt{1+\psi^2}K_{1/3}(\lambda),$$
$$J_n'(z_n) \approx \frac{1}{\sqrt{3}\pi}\frac{\varepsilon^2}{\sin^2\alpha}\big(1+\psi^2\big)K_{2/3}(\lambda),$$
$$\lambda = \frac{n}{3}\frac{\varepsilon^3}{\sin^3\alpha}\big(1+\psi^2\big)^{3/2}. \tag{14}$$

The integration boundaries in (2) can be extended to infinity, given the decay of the integrands. Assembling the enumerated approximations, we arrive at the transversal power coefficients,

$$P_n^{\mathrm{T}} \approx \frac{\alpha_{\mathrm{q}}}{3\pi^2}\frac{\varepsilon^5}{\sin^7\alpha}\frac{n^4\omega_{\mathrm{B}}^4}{n^2\omega_{\mathrm{B}}^2+m_{\mathrm{t}}^2\sin^4\alpha} \times\left[\int_{-\infty}^{+\infty}\psi^2\big(1+\psi^2\big)K_{1/3}^2\left(\frac{\xi}{2}\big(1+\psi^2\big)^{3/2}\right)d\psi + \mathrm{sign}^2(e)\int_{-\infty}^{+\infty}\big(1+\psi^2\big)^2K_{2/3}^2\left(\frac{\xi}{2}\big(1+\psi^2\big)^{3/2}\right)d\psi\right], \tag{15}$$

and the longitudinal coefficients read

$$P_n^{\mathrm{L}} \approx \frac{\alpha_{\mathrm{q}}}{3\pi^2}\frac{m_{\mathrm{t}}^2\varepsilon^3}{\sin^3\alpha}\frac{n^2\omega_{\mathrm{B}}^2}{n^2\omega_{\mathrm{B}}^2+m_{\mathrm{t}}^2\sin^4\alpha} \times\int_{-\infty}^{+\infty}\big(1+\psi^2\big)K_{1/3}^2\left(\frac{\xi}{2}\big(1+\psi^2\big)^{3/2}\right)d\psi. \tag{16}$$

Here, we defined

$$\xi := \frac{2n}{3}\frac{\varepsilon^3}{\sin^3\alpha}, \tag{17}$$

with ε in (10). The transversal power radiated in $\boldsymbol{\varepsilon}_\perp$-polarization is given by the $\mathrm{sign}^2(e)$ term, and the $\boldsymbol{\varepsilon}_\parallel$-polarized transversal radiation by the $K_{1/3}^2$-integration in (15). The integrals in (15) and (16) can be simplified by the identities [10,11]

$$\int_{-\infty}^{+\infty}\psi^2\big(1+\psi^2\big)K_{1/3}^2\left(\frac{\xi}{2}\big(1+\psi^2\big)^{3/2}\right)d\psi = \frac{\pi^2}{\xi}\big(F_\infty(\xi)-G_\infty(\xi)\big),$$
$$\int_{-\infty}^{+\infty}\big(1+\psi^2\big)^2K_{2/3}^2\left(\frac{\xi}{2}\big(1+\psi^2\big)^{3/2}\right)d\psi = \frac{\pi^2}{\xi}\big(F_\infty(\xi)+G_\infty(\xi)\big),$$
$$\int_{-\infty}^{+\infty}\big(1+\psi^2\big)K_{1/3}^2\left(\frac{\xi}{2}\big(1+\psi^2\big)^{3/2}\right)d\psi = \frac{2\pi^2}{\xi}L_\infty(\xi), \tag{18}$$

where the spectral functions on the right-hand side read

$$F_\infty(\xi) := \frac{1}{\sqrt{3}\pi}\int_\xi^\infty K_{5/3}(x)\,dx, \qquad G_\infty(\xi) := \frac{1}{\sqrt{3}\pi}K_{2/3}(\xi),$$
$$L_\infty(\xi) := \frac{1}{\sqrt{3}\pi}\int_\xi^\infty K_{1/3}(x)\,dx,$$
$$L_\infty(\xi) = 2G_\infty(\xi) - F_\infty(\xi). \tag{19}$$

The easiest way to derive these identities is to write $K_{1/3}$ and $K_{2/3}$ in terms of $\mathrm{Ai}(x)$ and its derivative, and then to use the standard integral representation for $\mathrm{Ai}(x)$, cf. Section 2.2.

The total power transversally and longitudinally radiated is obtained by summing over the individual modes, $P^{\mathrm{T,L}} = \sum_{n=1}^\infty P_n^{\mathrm{T,L}}$. We pass to continuous frequencies by identifying $\omega = \omega_n \approx \omega_{\mathrm{B}} n/\sin^2\alpha$, so that the continuous spectral densities read $p^{\mathrm{T,L}}(\omega) := P_n^{\mathrm{T,L}}\,dn/d\omega$, with $n = (\omega/\omega_{\mathrm{B}})\sin^2\alpha$. We find ξ in (17) as

$$\xi(\omega) = \kappa\frac{\omega_{\mathrm{b}}^2}{\omega^2}\big|\omega^2/\omega_{\mathrm{b}}^2-1\big|^{3/2},$$
$$\omega_{\mathrm{b}} := m_{\mathrm{t}}\gamma,\ \kappa := \frac{2}{3}\frac{m_{\mathrm{t}}}{\gamma^2\omega_{\mathrm{B}}\sin\alpha}. \tag{20}$$

This is $\xi(\omega)$ as in Ref. [1], rescaled by $1/\sin\alpha$.

The restriction $z < n$ on the Nicholson asymptotics (13) translates into $\omega > \omega_{\mathrm{b}}$. In this frequency band, we find the transversal density, cf. (15) and (18),

$$p^{\mathrm{T}}(\omega) = p_\parallel^{\mathrm{T}}(\omega) + \mathrm{sign}^2(e)\,p_\perp^{\mathrm{T}}(\omega), \tag{21}$$

$$p_{\parallel,\perp}^{\mathrm{T}}(\omega) = \frac{1}{2}\alpha_{\mathrm{q}}\frac{m_{\mathrm{t}}^2\omega}{\omega^2+m_{\mathrm{t}}^2}\left(\frac{\omega^2}{\omega_{\mathrm{b}}^2}-1\right)\big(F_\infty(\xi)\mp G_\infty(\xi)\big), \tag{22}$$

where ξ and ω_{b} are defined in (20). The lower plus-sign in (22) refers to the $\perp$-polarization. $p^{\mathrm{T}}(\omega)$ in (21) stands for the total transversal radiation; we have $\mathrm{sign}^2(e) = 1$. The longitudinal density is assembled with (16) and (18),

$$p^{\mathrm{L}}(\omega) = \alpha_{\mathrm{q}}\frac{m_{\mathrm{t}}^2\omega}{\omega^2+m_{\mathrm{t}}^2}L_\infty(\xi). \tag{23}$$

The spectral functions $F_\infty(\xi)$, $G_\infty(\xi)$, and $L_\infty(\xi)$ are defined in (19). The pitch angle enters in $p^{\mathrm{T,L}}(\omega)$ via the rescaled gyrofrequency, $\omega_{\mathrm{B}} \to \omega_{\mathrm{B}}\sin\alpha$, cf. (20).

2.2. Analytic continuation into the low-frequency band

Densities (21)–(23) can be continued into the low-frequency regime, $\omega \leqslant \omega_{\mathrm{b}}$, by means of Airy functions. The Airy repre-

sentation of the spectral functions (19) reads

$$L_\infty(\xi)=\int_z^\infty \mathrm{Ai}(x)\,dx,\qquad G_\infty(\xi)=-z^{-1}\mathrm{Ai}'(z), \tag{24}$$

where $z=(3\xi/2)^{2/3}$. We define the shortcut

$$\eta(\omega,\alpha):=\frac{\omega^{2/3}}{(\omega_\mathrm{B}\sin\alpha)^{2/3}}\left(1-\frac{\omega_\mathrm{b}^2}{\omega^2}\right)\frac{1}{\gamma^2}, \tag{25}$$

so that $\xi=(2/3)|\eta|^{3/2}$, cf. (20), and find

$$\begin{aligned}p^\mathrm{T}(\omega)&=p^\mathrm{T}_\parallel(\omega)+p^\mathrm{T}_\perp(\omega),\\ p^\mathrm{T}_{\parallel,\perp}(\omega)&=\frac{\alpha_\mathrm{q}}{2}\frac{m_\mathrm{t}^2\omega}{\omega^2+m_\mathrm{t}^2}\left(1-\frac{\omega^2}{\omega_\mathrm{b}^2}\right)\\ &\quad\times\left(\int_\eta^\infty \mathrm{Ai}(x)\,dx+(2\mp1)\frac{1}{\eta}\mathrm{Ai}'(\eta)\right),\end{aligned} \tag{26}$$

$$p^\mathrm{L}(\omega)=\alpha_\mathrm{q}\frac{m_\mathrm{t}^2\omega}{\omega^2+m_\mathrm{t}^2}\int_\eta^\infty \mathrm{Ai}(x)\,dx. \tag{27}$$

These densities coincide with (22) and (23) for $\omega\geqslant\omega_\mathrm{b}$, and they also constitute the analytic continuation into the lower frequency band $\omega\leqslant\omega_\mathrm{b}$, where $\eta(\omega,\alpha)$ is negative. The lower plus-sign in (26) refers to the $\perp$-polarization. The pitch angle enters only via $\eta(\omega,\alpha)$, cf. (25).

3. Pitch-angle averaging

We perform a pitch-angle average with density [11]

$$d\rho_\lambda(\alpha)=(\lambda+1)\sin^\lambda\alpha\cos\alpha\,d\alpha, \tag{28}$$

where $\lambda>-1$. This density is normalized to one over the interval $[0,\pi/2]$. The averaging is done by replacing $\int_\eta^\infty \mathrm{Ai}(x)\,dx$ in (26) and (27) with

$$\begin{aligned}\left\langle\int\mathrm{Ai}\right\rangle_\lambda&:=\int_0^{\pi/2}\int_{\eta(\omega,\alpha)}^\infty \mathrm{Ai}(x)\,dx\,d\rho_\lambda(\alpha)\\ &=\frac{3}{2}(\lambda+1)\int_1^\infty\int_{\eta_0 y}^\infty \mathrm{Ai}(x)\,dx\,y^{-(3\lambda+5)/2}\,dy\\ &=\int_{\eta_0}^\infty \mathrm{Ai}(x)\,dx-\eta_0\int_1^\infty \mathrm{Ai}(\eta_0 x)x^{-3(\lambda+1)/2}\,dx,\end{aligned} \tag{29}$$

and $\mathrm{Ai}'(\eta)/\eta$ in (26) is replaced by

$$\begin{aligned}\langle\mathrm{Ai}'\rangle_\lambda&:=\int_0^{\pi/2}\frac{\mathrm{Ai}'(\eta(\omega,\alpha))}{\eta(\omega,\alpha)}d\rho_\lambda(\alpha)\\ &=\frac{3(\lambda+1)}{2\eta_0}\int_1^\infty \mathrm{Ai}'(\eta_0 y)y^{-(3\lambda+7)/2}\,dy\\ &=\frac{3(\lambda+1)}{2\eta_0^2}\left(\frac{3\lambda+7}{2}\int_1^\infty \mathrm{Ai}(\eta_0 x)x^{-3(\lambda+3)/2}\,dx\right.\\ &\quad\left.-\mathrm{Ai}(\eta_0)\right).\end{aligned} \tag{30}$$

Here, $\eta_0(\omega):=\eta(\omega,\alpha=\pi/2)$, cf. (25), so that $\eta=\eta_0/\sin^{2/3}\alpha$. The averages (29) and (30) remain unaltered, if we replace the integration over $\int_0^{\pi/2}$ by $\int_\pi^{\pi/2}$. This also holds for the normalization of density (28), $\int_\pi^{\pi/2}d\rho_\lambda(\alpha)=1$. More generally, we may average over the full pitch-angle range $[0,\pi]$ with density

$$\begin{aligned}d\sigma_{A,\lambda_1,\lambda_2}(\alpha)&=A\theta\left(\frac{\pi}{2}-\alpha\right)d\rho_{\lambda_1}(\alpha)\\ &\quad-(1-A)\theta\left(\alpha-\frac{\pi}{2}\right)d\rho_{\lambda_2}(\alpha),\end{aligned} \tag{31}$$

where $\lambda_{1,2}>-1$ and $0\leqslant A\leqslant 1$. $d\rho_\lambda$ is defined in (28). The distribution (31) is normalized to one, $\int_0^\pi d\sigma_{A,\lambda_1,\lambda_2}(\alpha)=1$. Thus the averaging of the spectral densities (26) and (27) is effected by the substitutions

$$\begin{aligned}\int_\eta^\infty \mathrm{Ai}(x)\,dx&\to\int_0^\pi\int_\eta^\infty \mathrm{Ai}(x)\,dx\,d\sigma_{A,\lambda_1,\lambda_2}(\alpha)\\ &=A\left\langle\int\mathrm{Ai}\right\rangle_{\lambda_1}+(1-A)\left\langle\int\mathrm{Ai}\right\rangle_{\lambda_2},\end{aligned} \tag{32}$$

$$\begin{aligned}\frac{\mathrm{Ai}'(\eta)}{\eta}&\to\int_0^\pi\frac{1}{\eta}\mathrm{Ai}'(\eta)d\sigma_{A,\lambda_1,\lambda_2}(\alpha)\\ &=A\langle\mathrm{Ai}'\rangle_{\lambda_1}+(1-A)\langle\mathrm{Ai}'\rangle_{\lambda_2}.\end{aligned} \tag{33}$$

We denote the averaged densities by $\langle p^{\mathrm{T,L}}(\omega)\rangle_\sigma$.

The averages $\langle\int\mathrm{Ai}\rangle_\lambda$ and $\langle\mathrm{Ai}'\rangle_\lambda$ in (29) and (30) depend on ω only via $\eta_0(\omega)$, cf. after (30). We briefly discuss their $|\eta_0|\gg1$ asymptotics, starting with the low-frequency band, $\omega\leqslant\omega_\mathrm{b}$, cf. after (27), where η_0 is negative. In leading order,

$$\begin{aligned}&\mathrm{Ai}\big(-|\eta_0|\big)\\ &\quad=\frac{1}{\sqrt{\pi}|\eta_0|^{1/4}}\cos\left(\frac{2}{3}|\eta_0|^{3/2}-\frac{\pi}{4}\right)\big(1+\mathrm{O}\big(|\eta_0|^{-3/2}\big)\big),\end{aligned} \tag{34}$$

$$\begin{aligned}&\int_1^\infty \mathrm{Ai}\big(-|\eta_0|x\big)x^{-\beta}\,dx\\ &\quad=\frac{1}{\sqrt{\pi}|\eta_0|^{7/4}}\cos\left(\frac{2}{3}|\eta_0|^{3/2}+\frac{\pi}{4}\right)\big(1+\mathrm{O}\big(|\eta_0|^{-3/2}\big)\big),\end{aligned} \tag{35}$$

where $\beta\geqslant0$. The systematic asymptotic expansion of the integral (35) can be obtained by substituting the asymptotic series of the Airy function and applying term-by-term integration,

which results in a series of incomplete Γ-functions. The latter are then replaced by their asymptotic series. The leading order stated in (35) is independent of the exponent β, which enters linearly in the next-to-leading order; if β is large, we have to require $\beta/|\eta_0|^{3/2} \ll 1$ for the O-term to be small. In (29), we also need

$$\int_{-|\eta_0|}^{\infty} \mathrm{Ai}(x)\,dx = \frac{1}{3} + \int_0^{|\eta_0|} \mathrm{Ai}(-x)\,dx = 1 - \frac{1}{\sqrt{\pi}|\eta_0|^{3/4}} \cos\left(\frac{2}{3}|\eta_0|^{3/2} + \frac{\pi}{4}\right)\left(1 + \mathrm{O}\left(|\eta_0|^{-3/2}\right)\right). \tag{36}$$

Substituting the leading-order asymptotics (34)–(36) into the averages (29) and (30), we find

$$\left\langle \int \mathrm{Ai} \right\rangle_\lambda = 1 + \mathrm{O}\left(|\eta_0|^{-9/4}\right), \qquad \langle \mathrm{Ai}' \rangle_\lambda = \mathrm{O}\left(|\eta_0|^{-9/4}\right). \tag{37}$$

Thus the averaged spectral densities (as defined by (26) and (27) with substitutions (32) and (33)) converge for large $|\eta_0|$ to the densities generated by a charge in uniform motion, cf. Section 4, irrespectively of the choice of parameters in the pitch-angle distribution (31).

We turn to the upper frequency range, $\omega \geqslant \omega_\mathrm{b}$, where $\eta_0(\omega)$ is positive. The asymptotics of $\langle \int \mathrm{Ai} \rangle_\lambda$ and $\langle \mathrm{Ai}' \rangle_\lambda$ is obtained from

$$\mathrm{Ai}(\eta_0) \sim \frac{1}{2\sqrt{\pi}\,\eta_0^{1/4}} \exp\left(-\frac{2}{3}\eta_0^{3/2}\right),$$

$$\int_1^{\infty} \mathrm{Ai}(\eta_0 x) x^{-\beta}\,dx \sim \frac{1}{2\sqrt{\pi}\,\eta_0^{7/4}} \exp\left(-\frac{2}{3}\eta_0^{3/2}\right),$$

$$\int_{\eta_0}^{\infty} \mathrm{Ai}(x)\,dx = \frac{1}{3} - \int_0^{\eta_0} \mathrm{Ai}(x)\,dx \sim \frac{1}{2\sqrt{\pi}\,\eta_0^{3/4}} \exp\left(-\frac{2}{3}\eta_0^{3/2}\right). \tag{38}$$

The next-to-leading orders are by a factor of $\mathrm{O}(\eta_0^{-3/2})$ smaller, like in (34)–(36). We thus find, above the break frequency,

$$\left\langle \int \mathrm{Ai} \right\rangle_\lambda = \mathrm{O}\left(\eta_0^{-9/4} \exp\left(-\frac{2}{3}\eta_0^{3/2}\right)\right),$$

$$\langle \mathrm{Ai}' \rangle_\lambda = \mathrm{O}\left(\eta_0^{-9/4} \exp\left(-\frac{2}{3}\eta_0^{3/2}\right)\right). \tag{39}$$

The averaged spectral densities vanish for large (and even moderate) positive $\eta_0(\omega)$, reflecting the fact that the spectral densities of a charge in uniform motion vanish identically for $\omega \geqslant \omega_\mathrm{b}$, cf. Section 4.

The pitch-angle distribution $d\sigma_{A,\lambda_1,\lambda_2}(\alpha)$ is peaked in the interval $[0, \pi/2]$, at $\sin\alpha_{\mathrm{p}1} = \sqrt{\lambda_1/(\lambda_1+1)}$, provided that $\lambda_1 > 0$. If $-1 < \lambda_1 \leqslant 0$, it decreases monotonically to zero. The peak in the interval $[\pi/2, \pi]$ occurs at $\sin\alpha_{\mathrm{p}2} = \sqrt{\lambda_2/(\lambda_2+1)}$. If $-1 < \lambda_2 < 0$, the density increases in this interval from zero to infinity. For instance, $\lambda_{1,2} = 1$ gives $\alpha_{\mathrm{p}1} = \pi/4$; $\lambda_{1,2} = 1/3$ gives $\alpha_{\mathrm{p}1} = \pi/6$, and $\lambda_{1,2} = 3$ amounts to a peak at $\alpha_{\mathrm{p}1} = \pi/3$. The respective second peak in $[\pi/2, \pi]$ is obtained as $\alpha_{\mathrm{p}2} = \pi - \alpha_{\mathrm{p}1}$. If $A = 1/2$ and $\lambda_1 = \lambda_2$, the density is symmetric around $\alpha = \pi/2$. If $\lambda_{1,2} > 0$, it vanishes at the interval boundaries and $\pi/2$. These three pitch angles correspond to the limit cases of rectilinear motion parallel and antiparallel to the magnetic field, and to circular orbits orthogonal to **B**. If $\lambda_{1,2}$ is negative or close to zero, the average is dominated by pitch angles close to zero and π, so that the radiation density generated in uniform motion is prevalent. The latter is obtained by performing the zero-pitch-angle limit $\sin\alpha \to 0$ in (26) and (27), cf. Ref. [12] and Figs. 1 and 2. If $\lambda_{1,2} \gg 1$, the distribution (31) has two peaks close to $\pi/2$, even though it vanishes at $\pi/2$, so that the synchrotron densities (26) and (27) at $\sin\alpha \approx 1$ dominate the average.

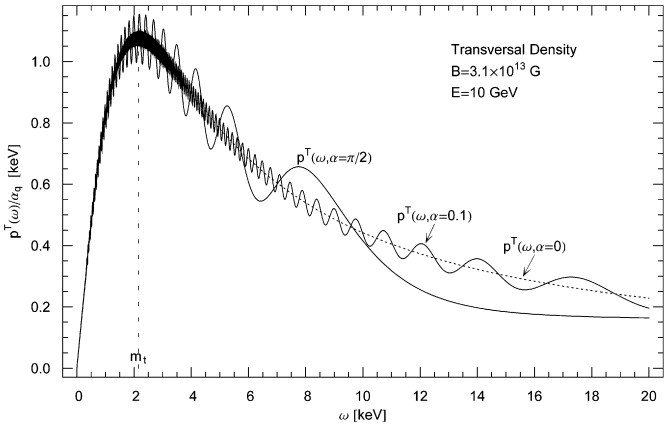

Fig. 1. Transversal tachyonic spectral density $p^\mathrm{T}(\omega)$, cf. (26), in the polar surface field, $B \approx 3.1 \times 10^{13}$ G, of the γ-ray pulsar PSR B1509–58, cf. Refs. [13–15]. The electronic orbital energy is 10 GeV. The density is shown for three pitch angles, $\alpha = \pi/2$ (circular orbit), $\alpha = 0.1$, and $\alpha = 0$. The latter corresponds to a charge in straight uniform motion, cf. (40). The radiation densities are rescaled with the tachyonic fine structure constant α_q, cf. after (2). The gyrofrequency is $\omega_\mathrm{B} \approx 18$ eV, the helical curvature radius $R \approx 1.1 \times 10^{-6}$ cm. The break frequency is $\omega_\mathrm{b} \approx 42$ MeV. The spectral peak is located at about the tachyon mass, 2 keV, followed by an extended X-ray tail with power-law decay, in contrast to the exponential cutoff in the upper frequency band, cf. (19).

The units $\hbar = c = 1$ can easily be restored. Gyroradius (magnetic bending radius, helical curvature radius) and gyrofrequency are connected by $R = c/\omega_\mathrm{B}$ in the ultra-relativistic regime. The length of one helical turn is $2\pi R$, and $R\sin\alpha$ is the radius of the helical base circle. Electronic energy and Lorentz factor are related as $\gamma \approx 1957E$ [GeV], so that ω_B [keV] $\approx 5.9 \times 10^{-15} B$ [G]$/E$ [GeV] and R [cm] $\approx 2.0 \times 10^{-8}/\omega_\mathrm{B}$ [keV], and the tachyonic break frequency scales as ω_b [keV] $\approx 4.2 \times 10^3 E$ [GeV]. Figs. 1–3 illustrate the pitch-angle scaling and averaging of the superluminal radiation densities of ultra-relativistic electrons orbiting in the polar field of a γ-ray pulsar.

4. Tachyonic spectral fit to the γ-ray broadband of the binary pulsar PSR B1259–63

To compare to observational spectral maps, we have to perform a further average over the electron density [2]. We demon-

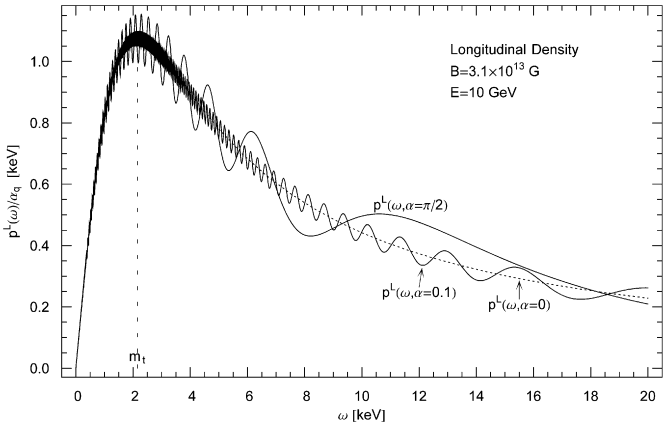

Fig. 2. Longitudinal spectral density $p^{\mathrm{L}}(\omega)$, cf. (27). Magnetic field, electron energy and pitch angles as in Fig. 1. The oscillations are superimposed by the magnetic field and vanish at zero pitch angle, for rectilinear motion along the magnetic field lines. The transversal and longitudinal spectral densities of a uniformly moving ultra-relativistic electron (dotted curve in Figs. 1 and 2) coalesce in the depicted frequency range, $\omega \ll \omega_{\mathrm{b}}$.

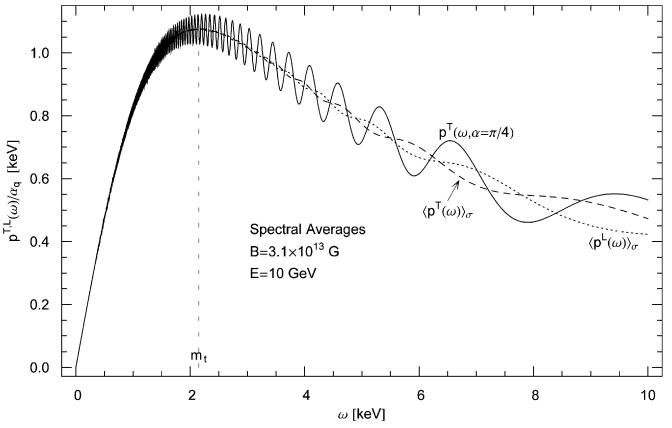

Fig. 3. Transversal and longitudinal spectral densities $\langle p^{\mathrm{T,L}}(\omega)\rangle_\sigma$, averaged with the symmetric pitch-angle distribution $d\sigma(A = 1/2, \lambda_1 = \lambda_2 = 1)$, cf. (31). This distribution is peaked at pitch angles of 45° and 135°, in the cross-over region between the synchrotron regime and rectilinear motion. Magnetic field and orbital energy as in Figs. 1 and 2. For comparison, we also indicate the unaveraged transversal distribution $p^{\mathrm{T}}(\omega)$ at these pitch angles, $\sin\alpha = 1/\sqrt{2}$; the modulations are wiped out by the averaging.

strated that a pitch-angle average attenuates the modulations in the spectral slope, cf. Fig. 3, so that the synchrotron densities approach the spectral densities of a uniformly moving charge,

$$p^{\mathrm{T,L}}(\omega,\gamma) = \frac{\alpha_{\mathrm{q}} m_{\mathrm{t}}^2 \omega}{\omega^2 + m_{\mathrm{t}}^2}\left[\gamma^2 - \left(1 + \frac{\omega^2}{m_{\mathrm{t}}^2}\right)\Delta^{\mathrm{T,L}}\right]\frac{1}{\gamma\sqrt{\gamma^2-1}}, \tag{40}$$

where $\Delta^{\mathrm{T}} = 1$ and $\Delta^{\mathrm{L}} = 0$ for the transversal and longitudinal radiation component, respectively. The spectral cutoff occurs at $\omega_{\max}(\gamma) := m_{\mathrm{t}}\sqrt{\gamma^2-1}$, to be identified with the break frequency ω_{b} in the ultra-relativistic limit, cf. (20). Only frequencies in the range $0 < \omega < \omega_{\max}(\gamma)$ can be radiated by a uniformly moving charge [16].

We average with electronic power laws exponentially cut with a Boltzmann density, $d\rho \propto E^{-2-\alpha} e^{-E/(kT)}\, d^3p$. Parametrized with the Lorentz factor, this reads

$$d\rho_{\alpha,\beta}(\gamma) = A_{\alpha,\beta}\gamma^{-\alpha-1}e^{-\beta\gamma}\sqrt{\gamma^2-1}\,d\gamma. \tag{41}$$

The normalization $A_{\alpha,\beta}$ is determined by $n_1 = A_{\alpha,\beta} \times \int_{\gamma_1}^{\infty} d\rho_{\alpha,\beta}(\gamma)$, where n_1 is the electron count and γ_1 the smallest Lorentz factor of the source population. $\beta = mc^2/(kT)$, and α is the electronic power-law index (not to be confused with the pitch angle). Here, we consider thermal distributions, defined by $\alpha = -2$ and $\gamma_1 = 1$. The average is carried out as [2]

$$\big\langle p^{\mathrm{T,L}}(\omega)\big\rangle_{\alpha,\beta} := \int_{\gamma_1}^{\infty} p^{\mathrm{T,L}}(\omega,\gamma)\theta\big(\omega_{\max}(\gamma)-\omega\big)\,d\rho_{\alpha,\beta}(\gamma). \tag{42}$$

The spectral fit is based on the E^2-rescaled flux density $dN^{\mathrm{T,L}}/dE$, which is related to the averaged energy density by

$$E^2\frac{dN^{\mathrm{T,L}}}{dE} = \frac{\omega}{4\pi d^2}\big\langle p^{\mathrm{T,L}}(\omega)\big\rangle_{\alpha,\beta}, \tag{43}$$

where d is the distance to the pulsar. In Figs. 4–6, we plot the flux density of two thermal electron populations $\rho_{1,2}$ specified in Table 1. Each electron density generates a cascade ρ_i, the wideband spectral map is obtained by adding the cascade spectra.

As for the electron count n_1, it is convenient to use a rescaled parameter $\hat{n}_1$ for the fit,

$$\hat{n}_1 := \frac{\alpha_{\mathrm{q}} n_1}{\hbar\ [\mathrm{keV\,s}]4\pi d^2\ [\mathrm{cm}]} \approx 1.27\times 10^{-39}\frac{n_1}{d^2\ [\mathrm{kpc}]}, \tag{44}$$

which is independent of the distance estimate. Here, $\hbar$ [keV s] implies the tachyon mass in keV units, that is, we put $m_{\mathrm{t}} \approx 2.15$ in the spectral density (40). At γ-ray energies, only a tiny $\alpha_{\mathrm{q}}/\alpha_{\mathrm{e}}$-fraction (the ratio of tachyonic and electric fine structure constants) of the tachyon flux is actually absorbed by the detector [17], which requires a rescaling of the electron count n_1, so that the actual number of radiating electrons is $n_1^{\mathrm{e}} := n_1\alpha_{\mathrm{e}}/\alpha_{\mathrm{q}} \approx 7.3\times 10^{10} n_1$. We thus find the electron count as $n_1^{\mathrm{e}} \approx 5.7\times 10^{49}\hat{n}_1 d^2$ [kpc], where $\hat{n}_1$ is determined by the tachyonic flux amplitude obtained from the spectral fit. Finally, electron temperature and cutoff parameter in the electronic Boltzmann factor are related as kT [TeV] $\approx 5.11\times 10^{-7}/\beta$.

Figs. 4–6 show the least-squares fit to the γ-ray wideband of the binary system PSR B1259–63/SS 2883, cf. Refs. [18–24]. The extended spectral plateau as well as the spectral curvature over the entire frequency range can readily be reproduced by a tachyonic cascade spectrum. (As for the high-magnetic-field pulsar PSR B1509–58, cf. Figs. 1–3, there are currently not enough data points available for a spectral fit [14]. A tachyonic spectral fit to the pulsed Crab flux is given in Ref. [25], where the spectral asymptotics of the averaged densities and the technical details of the nonlinear χ^2-fit are discussed as well.) We assume $d \approx 1.5$ kpc as distance to the pulsar, based on optical and scintillation observations [22], although it could be as high as 4.5 kpc if inferred from the dispersion measure [23]. In the latter case, the electronic source count has to be rescaled accordingly, $n_1^{\mathrm{e}} \propto d^2$; the spectral maps are not affected by the distance estimate. The total flux above 380 GeV is 5% of the

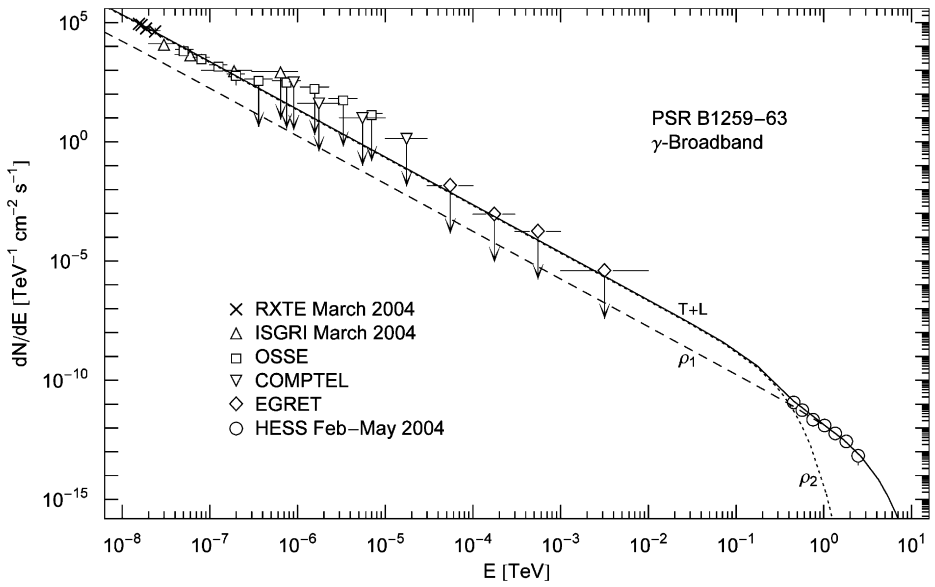

Fig. 4. γ-ray wideband of the binary pulsar PSR B1259–63. RXTE and ISGRI data points from [18], OSSE points from [19], COMPTEL and EGRET upper limits from [20], HESS points from [21]. The solid line T + L is the unpolarized differential tachyon flux $dN^{\mathrm{T+L}}/dE$, obtained by adding the flux densities $\rho_{1,2}$ of two thermal electron populations. The χ^2-fit is based on the first three ISGRI points, the first four OSSE points, and the HESS points. The fourth ISGRI point, the remaining five OSSE points, as well as the COMPTEL and EGRET points are upper limits only. The four depicted RXTE points are at the upper edge of the hard X-ray spectrum detectable with the RXTE proportional counter [18], they suggest a seamless transition into the X-ray band, but have not been included in the least-squares fit.

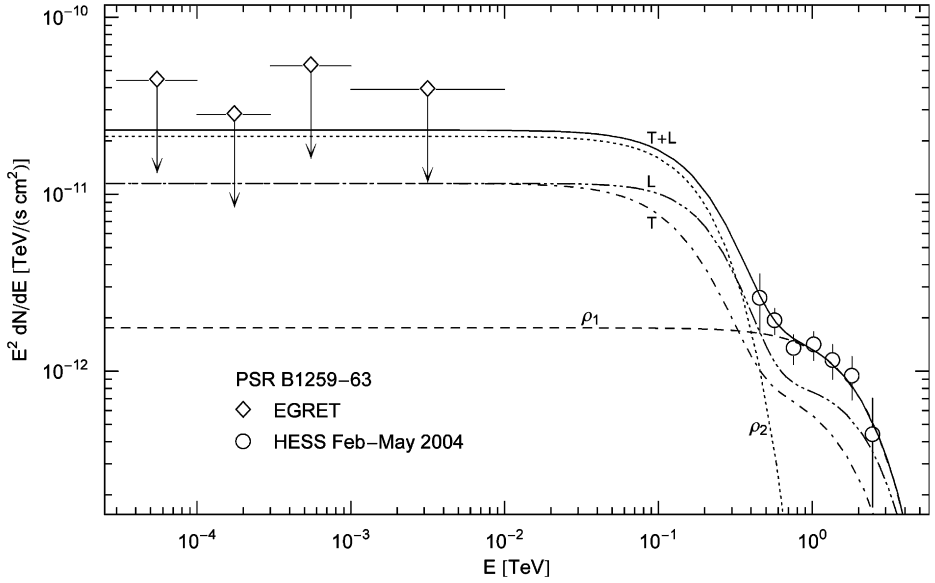

Fig. 5. EGRET plateau and HESS slope of PSR B1259–63. The solid line T + L is the unpolarized tachyon flux $dN^{\mathrm{T+L}}/dE$ rescaled with E^2 to render the spectral curvature visible. The latter is caused by the Boltzmann factor in the averaged spectral densities (42); the exponential decay of the cascades $\rho_{1,2}$ sets in at about $E_{\mathrm{cut}} \approx (m_{\mathrm{t}}/m)kT$, implying cutoffs at 0.8 TeV for the ρ_1-cascade and 80 GeV for ρ_2. The unpolarized flux T + L can be split into transversal (dot-dashed) and longitudinal (dot-dot-dashed) components $dN^{\mathrm{T,L}}/dE$, cf. (43). The spectral plateau extends from the ISGRI and OSSE points in the keV range to the first spectral cut at 80 GeV, cf. Fig. 4.

unpulsed Crab flux [21]. The electronic source count for the Crab pulsar at 2 kpc is 2.6×10^{49}, cf. Ref. [25], as compared to 3.2×10^{47} for PSR B1259–63, cf. Table 1.

Several electromagnetic radiation mechanisms have been invoked to model the spectra of γ-ray pulsars, most notably curvature radiation due to electric fields followed by pair creation, accompanied by synchrotron radiation and inverse Compton scattering [26]. An electromagnetic spectral fit to the γ-ray wideband of the PSR B1259–63/SS 2883 binary was performed in Ref. [20], in the context of a synchro–inverse-Compton model; the tachyonic wideband fit in Fig. 4 is directly comparable to Fig. 16 of this reference. The tachyonic TeV fit in Fig. 6 is directly comparable to the inverse-Compton fit in Fig. 15 of Ref. [24].

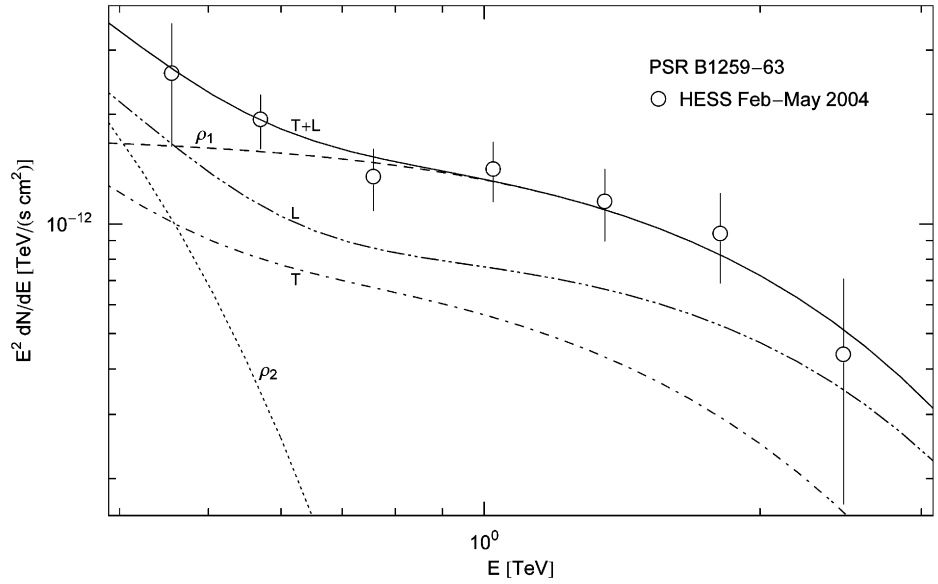

Fig. 6. Close-up of the HESS spectrum of PSR B1259–63 in Fig. 5. The tachyon flux T + L is obtained by adding the cascades $\rho_{1,2}$. The TeV spectral map coincides with the ρ_1-cascade, since the ρ_2-flux is exponentially cut at 80 GeV, cf. Fig. 5. Temperature and source number of the electron populations generating the cascades are listed in Table 1.

Table 1
Thermal electronic source densities $\rho_{1,2}$ generating the γ-ray broadband of the binary pulsar PSR B1259–63

	$\hat{n}$	β	n^{e}	kT (TeV)
ρ_1	1.9×10^{-4}	2.69×10^{-9}	2.4×10^{46}	190
ρ_2	2.3×10^{-3}	2.69×10^{-8}	2.95×10^{47}	19

The cascades $\rho_{1,2}$ in Figs. 4–6 are obtained by averaging the superluminal radiation densities with electron populations, cf. (42), which are in turn inferred from the spectral fit. Each distribution is defined by electron temperature kT and source count n^{e}, the latter based on a distance estimate of 1.5 kpc. β is the cutoff parameter in the electronic Boltzmann factor. $\hat{n}$ is the normalized amplitude of the tachyonic flux density defined in (44). The parameters $\hat{n}$ and β are extracted from the χ^2-fit.

5. Conclusion

We have studied superluminal radiation from ultrarelativistic electrons helically orbiting in strong magnetic fields and derived the pitch-angle scaling of the radiation densities. In the zero-magnetic-field limit, the tachyonic synchrotron densities converge to the spectral densities (40) for uniform motion. Orbital curvature induces modulations along the spectral slopes. If integrated over the pitch angles, these oscillations are averaged out, cf. Figs. 1–3.

We demonstrated that the γ-broadband of the binary pulsar PSR B1259–63 can be reproduced by a tachyonic cascade spectrum, cf. Figs. 4–6. The cascades are obtained by averaging the radiation densities with thermal electron distributions. At γ-ray energies, the speed of tachyons is close to the speed of light; the basic difference to electromagnetic radiation is the longitudinally polarized flux component. The polarization of tachyons can be determined from transversal and longitudinal ionization cross-sections of Rydberg atoms, which peak at different scattering angles [27].

We have focused on the γ-ray spectrum, including the high end of the X-ray tail. At X-ray energies, if a grating spectrometer is used [28], the interference peaks are determined by wavelength. In this case, the data points have to be reparametrized by wavelength, and then the tachyonic dispersion relation is substituted (which substantially differs from the photonic counterpart due to the 2 keV tachyon mass located in the X-ray regime) to obtain the tachyonic energy-flux relation. Tachyonic spectral fits in the X-ray band will be discussed elsewhere.

Acknowledgements

The author acknowledges the support of the Japan Society for the Promotion of Science. The hospitality and stimulating atmosphere of the Centre for Nonlinear Dynamics, Bharathidasan University, Trichy, and the Institute of Mathematical Sciences, Chennai, are likewise gratefully acknowledged.

References

[1] R. Tomaschitz, Physica A 335 (2004) 577.
[2] R. Tomaschitz, Ann. Phys. 322 (2007) 677.
[3] K. Nakagawa, et al., J. Electron Spectrosc. Relat. Phenomena 144 (2005) 271.
[4] K. Yagi-Watanabe, et al., Nucl. Instrum. Methods Phys. Res. A 553 (2005) 620.
[5] I.H. Suzuki, et al., Radiat. Phys. Chem. 75 (2006) 1778.
[6] Y. Morishita, et al., J. Phys. B 39 (2006) 1323.
[7] Y. Zou, et al., J. Phys. B 39 (2006) 4775.
[8] M. Oura, et al., Radiat. Phys. Chem. 76 (2007) 469.
[9] R. Tomaschitz, Eur. Phys. J. D 32 (2005) 241;
R. Tomaschitz, Eur. Phys. J. B 17 (2000) 523.
[10] A.A. Sokolov, I.M. Ternov, Radiation from Relativistic Electrons, Hilger, Bristol, 1986.
[11] V.L. Ginzburg, S.I. Syrovatskii, Annu. Rev. Astron. Astrophys. 7 (1969) 375;
K.C. Westfold, Astrophys. J. 130 (1959) 241.
[12] R. Tomaschitz, Eur. Phys. J. C 45 (2006) 493;
R. Tomaschitz, Astropart. Phys. 23 (2005) 117.
[13] S. Gunji, et al., Astrophys. J. 428 (1994) 284.

[14] L. Kuiper, et al., Astron. Astrophys. 351 (1999) 119.
[15] T. Sako, et al., Astrophys. J. 537 (2000) 422.
[16] R. Tomaschitz, Physica A 320 (2003) 329.
[17] R. Tomaschitz, Eur. Phys. J. C 49 (2007) 815.
[18] S.E. Shaw, et al., Astron. Astrophys. 426 (2004) L33.
[19] J.E. Grove, et al., Astrophys. J. 447 (1995) L113.
[20] M. Tavani, J. Arons, Astrophys. J. 477 (1997) 439.
[21] F. Aharonian, et al., Astron. Astrophys. 442 (2005) 1.
[22] N.M. McClure-Griffiths, et al., Astrophys. J. 492 (1998) L49.
[23] M. Chernyakova, et al., Mon. Not. R. Astron. Soc. 367 (2006) 1201; T.W. Connors, et al., Mon. Not. R. Astron. Soc. 336 (2002) 1201.
[24] D. Khangulyan, et al., astro-ph/0605663.
[25] R. Tomaschitz, Astropart. Phys. 27 (2007) 92.
[26] K. Hirotani, Adv. Space Res. 35 (2005) 1085.
[27] R. Tomaschitz, J. Phys. A 38 (2005) 2201.
[28] C.R. Canizares, et al., Publ. Astron. Soc. Pac. 117 (2005) 1144.